

Analyst

Accepted Manuscript



This is an *Accepted Manuscript*, which has been through the Royal Society of Chemistry peer review process and has been accepted for publication.

Accepted Manuscripts are published online shortly after acceptance, before technical editing, formatting and proof reading. Using this free service, authors can make their results available to the community, in citable form, before we publish the edited article. We will replace this *Accepted Manuscript* with the edited and formatted *Advance Article* as soon as it is available.

You can find more information about *Accepted Manuscripts* in the [Information for Authors](#).

Please note that technical editing may introduce minor changes to the text and/or graphics, which may alter content. The journal's standard [Terms & Conditions](#) and the [Ethical guidelines](#) still apply. In no event shall the Royal Society of Chemistry be held responsible for any errors or omissions in this *Accepted Manuscript* or any consequences arising from the use of any information it contains.



Analyst

PAPER

Deformability and size-based cancer cell separation using an integrated microfluidic device†

Received 00th January 20xx,
Accepted 00th January 20xx

DOI: 10.1039/x0xx00000x

www.rsc.org/

Long Pang,^a Shaofei Shen,^a Chao Ma,^a Tongtong Ma,^a Rui Zhang,^b Chang Tian,^a Lei Zhao,^a Wenming Liu^a and Jinyi Wang*^a

Cell sorting by filtration technique offers a label-free approach for cell separation on the basis of size and deformability. However, the filtration is always limited by the unpredictable variation of the filter hydrodynamic resistance due to cell accumulation and clogging in the microstructures. In this study, we present a new integrated microfluidic device for cell separation based on cell size and deformability by combining the microstructure-constricted filtration and pneumatic microvalves. Using this device, the cell populations sorted by the microstructures can be easily and real time released for subsequent analysis. Moreover, the periodical sort and release of cells greatly avoided cell accumulation and clogging and improved the selectivity. Separation of cancer cells (MCF-7, MDA-MB-231 and MDA231-LM2) with different deformability showed that the mixture of the less flexible cells (MCF-7) and the flexible cells (MDA-MB-231 and MDA231-LM2) can be well separated with more than 75% purity. Moreover, the device can be used to separate cancer cells from the blood samples with more than 90% cell recovery and more than 80% purity. Compared with the current filtration methods, the device provide a new approach for cancer cell separation with high collection recovery and purity, also, it possesses practical potential to be applied as a sample preparation platform for fundamental studies and clinical applications.

Introduction

More and more researches have shown that the biomechanical properties (deformability and size) of cells play an important role for their biological characteristics and function.¹⁻³ For example, less differentiated stem cells, which have greater deformability than the differentiated stem cells, have the potential to be induced more kinds of terminally differentiated cells (e.g. adipogenic, osteogenic, chondrogenic and myogenic lineages). Therefore, these cells, possibly producing more organs and tissues, have great medical value.⁴ Furthermore, the deformability and size of cancer cells have important effect on cancer diagnosis and therapy.⁵ Some low-abundance rare cells, such as circulating tumor cells (CTCs), are found in the peripheral blood of cancer patients, which is highly correlated with cancer metastasis.⁶ Almost cancer-related deaths are caused by cancer metastasis.⁷ Studies on cancer cell deformability consistently revealed that increased deformability is correlated with increased metastatic potential.^{8,9} In other words, the flexible CTCs are more threatening than the rigid CTCs. Therefore, the deformability and size of cells are

significant on biological research and clinical application.⁵ However, challenges remain existence for the separation of cells with different deformability and sizes.¹⁰

Traditionally, the methods used for the separation of cells with different deformability and sizes include affinity capture and non-affinity capture.^{11,12} Affinity capture uses chemical modification or labelling special cell markers (e.g. cellular nucleoskeleton protein and actin filaments) to separate cells. However, this kind of separation methods has influence on the biological property of the separated cells, giving rise to the inconvenience of subsequent studies.¹³ Moreover, affinity capture is unreliable when the cell surface markers used are absent on a portion of the target cells, which may miss some potentially valuable cells.¹⁴ Cell separation with non-affinity capture is the method that separates cells through the differences of cell biomechanical properties (deformability and size), such as atomic force microscope, magnetic twisting rheometry, micropipette aspiration and other derivatives.¹⁵⁻¹⁸ Although these non-affinity approaches do not relate to the special cell markers, they are complex in operation and expensive.⁵ Therefore, the development of simple, low cost and more efficient techniques for cell separation remains necessary for biological and medicine researches.¹⁰

As the development of microfluidic technology, methods for cell separation based on deformability and sizes are being developed.¹⁹ Generally, the current microfluidic approaches used for cell separation mainly include dielectrophoresis,^{20,21} hydrodynamic techniques,^{4,22-24} and filtration methods.²⁵⁻³⁰ Dielectrophoresis-based methods can achieve high-separation purity of cells

^a Colleges of Veterinary Medicine and Science, Northwest A&F University, Yangling, Shaanxi 712100, P. R. China. Fax: +86-298-708-2520; Tel: +86-298-708-2520; E-mail: jywang@nwsuaf.edu.cn

^b Department of Biochemistry & Biophysics, Texas A&M University College Station, TX 77843, USA.

† Electronic Supplementary Information (ESI) available: Materials and methods, supplementary Figs. S1–S19, Movies S1–S5 and Tables S1. See DOI: 10.1039/x0xx00000x

(typically >90%).^{20,21} Compared to filtration and hydrodynamic methods, dielectrophoresis-based methods usually lag in throughput (typically, <1 mL/h).²⁰ To improve the throughput, dielectrophoresis-based sorting techniques combined with other methods have been proposed. However, adopting a multi-step separation method can accumulate loss of the target cells in each step, which may decrease recovery of the target cells.²¹ Hydrodynamic methods can typically achieve high throughput (typically, >3 mL/h),^{4,22} however, its selectivity is often lower (the purity of the target cells is less than 50% in many cases²²⁻²⁴) than the filtration-based methods. Filtration techniques, which consist of microstructures or pore arrays, can separate and capture different cells based on size and deformability. The purity of the target cells often more than 70% in many cases,²⁵⁻³⁰ and the throughput could be increased by adding the number of filtration units (typically, >2 mL/h).^{27,28} The main challenge of filtration-based method is the potential for clogging when large numbers of cells are processed, which can result in irregular flows and low separation efficiency. Specifically, as the pores of filters were gradually blocked by the trapped cells, the hydrodynamic resistance of the filters changes unpredictably, resulting in the functional filter reducing and the separation efficiency decreasing.³¹ In addition, captured cells cannot be easily extracted from the filters or microstructures in some filtration devices, limiting the subsequent research of the captured cells such as genomic and protein analysis.³²

In this study, we design an integrated microfluidic device for physical separation of cells through the combination of a funnel-like filter matrix with the microvalve system.³¹ The device can capture and release cells repeatedly, which greatly improves its scalability without compromising its selectivity. Using this device, two kinds of cell samples were separated: (i) mixture of two types of cancer cells [mesenchymal-like cells (MDA-MB-231 or MDA231-LM2) and epithelium-like cells (MCF-7)] with different deformability; (ii) MDA-MB-231, MDA231-LM2 or MCF-7 cells spiked in blood samples with a cancer cell-to-blood cell ratio of 1/10⁶. The results demonstrate that the device has high selectivity and recovery rate for the separation of cancer cells with different deformability as well as the rare cancer cells in the blood samples. Moreover, the device can also allow easy retrieval of the target cells with high viability, which is of benefit for the downstream experiments.

Design

Filter unit

To improve cell separation efficiency and viability, the filter should be designed to avoid cell clogging and injury.³¹ In this work, a new architecture as a funnel-like filter unit was designed to avoid cell damage and improve the separation rate. As shown in Fig. S1 (ESI†), each filter unit consists of two semicircles and a rectangle, and the two neighbouring filter units form a funnel-like architecture with a minimum cross-sectional area (30°) for cell capture. The depth of the filter unit is 25 μm, which accommodates the typical mammalian cells in suspension.⁵ Numerical simulation (Fig. S2, ESI†) of the flow through the filter units showed that the velocity steeply reached

a peak at the minimum cross-sectional area (the pore) of the funnel and then gradually declined. This phenomenon provides a well-controlled hydrodynamic environment for cell capture or passing, avoiding the potential risk of clogging or cell damage caused by the prolonged contact between the cells and the filters.³²

Cell separation device

The prototype (Fig. 1) of the cell separation device consists of the filtration constriction arranged in a 2D array with 8-group filter matrices, and the membrane microvalves used to control the flows through the filter matrices in the horizontal direction for cell infusion and sort as well as to facilitate cell release in the vertical direction. The detailed design and dimensions of the device were shown in Fig. 1A. Fig. 1B is an actual image of the cell separation device. Specially, the microfluidic device was composed of four layers (Fig. S3A, ESI†) and was fabricated by PDMS using multilayer soft lithography technique.³³ For the detailed information on the preparation, see the electronic supplementary information (ESI†). The fluidic layer, with a micrometer-scaled fluid network, contained 8-group filter matrices for cell capture and sorting. The pore size of the funnel-like filter is constant in each matrix, but decreases in the subsequent matrices with a decrement of 2 μm from 20 to 6 μm; each matrix has 250-500 pores for cell separation. The cell inlet and waste outlet were designed for cell sample introduction and waste exclusion. L1, L2 and L3 channels were used for the buffer (PBS, 0.01 mol/L, PH 7.4; citric acid, 4.8 g/L; trisodium citrate, 13.2 g/L; and dextrose, 14.7 g/L) infusion which can drive the cell samples to pass through the filter matrices or the sorted cells to go out the device. The branching structure of the L1 and L3 channels was designed to obtain a stable and continuous microflow.³¹ The L4 and L5 channels were designed to facilitate the work of L1 and L3 when needed during cell introduction or exclusion.²⁸ In the control layer, eight big and parallel microvalves (the long and vertical red rectangles in Fig. 1A) located between the two adjacent filter matrices can intentionally regulate the opening and closing of the channels embedded in the fluidic layer to control the release of the sorted cells. The twelve small valves (the small red rectangles in Fig. 1A) and the two horizontal valves (the long and horizontal red rectangles in Fig. 1A) surrounding each chamber could regulate intentionally the opening and closing of the thin channels in the fluidic layer to allow cell sample delivery, waste exclusion and cell release. Each channel in the control layer was independently controlled by an external solenoid valve that can be modulated manually or automatically (see ESI†). The thin PDMS layer was employed to better withstand high actuation pressure for valves after irreversible bonding with the control layer, instead of reversible bonding directly between the control layer and the glass slide.³⁴

Operation cycle

The cell separation device operates on a repeating three-step cycle of infusion, sorting and exclusion (Fig. 1C, Fig. S3B and Fig. S4, ESI†). In the cell infusion and sorting steps, the cell sample was introduced from the cell inlet and pushed through

the funnel-like filter matrices by the buffer from L1 channel under a stable and continuous microflow,^{28,30,31} during which the sixteen vertical fluidic channels on both sides of the filter matrices were closed by regulating the corresponding valves; all the valves located between the two adjacent filter matrices were opened to allow the cell sample flow through the filter matrices for cell sorting according to their size and deformability. When the fluid containing fragile cells was pushed through the funnel-like filter matrices, it is critical that the pressure drop (ΔP), generally, a low pressure should be applied during the funnel-like filter matrices to avoid the stress induced cellular damage, however, too low pressure could not separate the cell with different size and deformability.³⁴ In the current experiments, the pressure drop was controlled by the driving buffer from L1 channel with a syringe pump (Longer pump, LSP01-1A). Considering a Newtonian fluid through a constant geometry of funnel-like filter matrices, the pressure can be calculated by the equation (Eq. 1) as follows.³¹

$$\Delta P \approx \frac{12\mu L}{wh^3} Q \quad (\text{Eq. 1})$$

where $w > h$, ΔP is the pressure drop, Q is the volumetric flow rate, μ is the viscosity of the fluid; w , h and L are the width, depth and length of the channel. For the given constant geometry area (1500 μm wide, 25 μm high and 7000 μm long), ΔP increases with Q .

In the cell exclusion step, the outlet channels for cell release were opened and the sorted cells were sequentially pushed into their own outlet channel by the buffer from the L2 and L3 channels under the help of the microvalve system. After all the sorted cells were extracted, the new cell sample was introduced into the device again for another separation and sorting. This operation cycle could be repeated indefinitely to increase the throughput of the separation process.

To demonstrate the operation of the three-step cycle, an example of the infusion of two different food-dye solutions (red and blue for easy visualization) were first performed in the microdevice (Fig. S5, ESI†). Briefly, the red flow, simulating the cell suspension, was first infused into the fluidic channels and pushed it through the filter matrices (Movie S1, ESI†). Then, the blue food-dye solution was infused into the fluidic channel from the reverse direction and released through the outlet by regulating the corresponding microvalves (Movie S2, ESI†), which simulated the process of cell release. The tests preliminary demonstrate that the integrated microfluidic device could realize cell infusion, sorting and controllable release in a fast, orderly and efficient manner.

Experimental

More detailed information on the materials and methods used can be found in the ESI†.

Cell sample preparation

In this study, three different types of human cancer cell lines were used to investigate the capacity of the microdevice to

separate cells based on their biomechanical properties. MCF-7 and MDA-MB-231 cell lines were obtained from the Chinese Academy of Sciences (Shanghai, China), and the lung-metastatic derivative MDA231-LM2 cell line was kindly provided by Professor Joan Massagué at the Memorial Sloan-Kettering Cancer Center, USA. The cancer cells were routinely cultured using Dulbecco's modified Eagle's medium (DMEM, Invitrogen, Grand Island, NY) supplemented with 10% fetal bovine serum (FBS, Invitrogen), 100 units/mL penicillin, and 100 mg/mL streptomycin in a humidified atmosphere of 5% CO_2 at 37 °C. To maintain cells in the exponential growth phase, they were normally passaged at a ratio of 1:3 every 72 h. To minimize sampling errors between the cells with different deformability, especially the size errors of cells caused by cell cycle, the cells were first grown in serum-free medium for 48 h before use.^{5,34} Afterward, the culture medium (the DMEM supplemented with 10% FBS) was removed and the cells were collected by centrifugation at 200×g for 5 min after washing twice with phosphate-buffered saline (PBS, 0.01 mol/L, pH 7.4) and treating with trypsin for 10 min.²⁶ To facilitate the observation during cell separation, these cancer cells were then stained with different fluorescence dyes following the method reported previously.³² Briefly, MCF-7 cells were gently re-suspended in a pre-warmed Cell Tracker Green CMFDA solution to stain for 30 min in a humidified atmosphere with 5% CO_2 at 37 °C. Using the same method, MDA-MB-231 and MDA231-LM2 cells were respectively stained using Cell Tracker Orange CMRA.

Cell separation

Prior to each experiment, the device was first sterilized by sequential rinsing with 70% alcohol, followed by Millipore ultrapure water and PBS. Then, a solution of 1% BSA in PBS was introduced into the device and incubated for 30 min to block the nonspecific adsorption of cells onto the channel surfaces.^{5,31,32} After rising again with PBS, cell infusion and sorting were performed at room temperature and coordinated with the actuation of the corresponding microvalves under different air pressures (0 psi to 20 psi). For the separation of cell mixtures with different deformability, the cell suspension with a cell density of 1×10^6 cells/mL were firstly infused into the device in 1–2 s from the cell inlet at a flow rate of 60 $\mu\text{L}/\text{min}$ to load 1 000 to 2 000 cells. Then, the cell inlet was closed by activating the corresponding valve and the driving buffer from the L1 channels pushed the cells through the filter matrices using a syringe pump. When the cells were stably distributed in their own filter matrices, the sorted cells were sequentially pushed out the device from their own outlets under the help of the microvalves. For the separation of cancer cells from blood samples, the blood samples were infused into the device from cell inlet at a constant flow rate. Meanwhile, the driving buffer from the L1 channel was infused into the device. The use of the driving buffer in this experiment could not only push the cells contained in the blood samples through the filter matrices, but also dilute the blood samples, allowing to process high haematocrit blood samples.²² After that, the cancer cells spiked in the whole blood were trapped in the filter matrices

and were sequentially pushed out the device from their own outlets under the help of the corresponding microvalves.

Cell viability assay

Cell viability before and after experiment was assessed via AO/PI double staining protocol and re-culturing.^{24,32} In detail, the AO/PI (5 µg/mL in PBS) staining solution was introduced into the cell samples and stained 10 min at room temperature after removing the growth medium and rinsing with PBS. Then, PBS was introduced for 5 min as a final rinse. The cells were imaged and enumerated for assessing the percentage of cell viability. To further evaluate the viability of the sorted cells, the recovered cells were re-cultured and their viability was compared with those cultured using the common bench top method.

Immunocytochemistry

The recovered cells were first attached on a round and polylysine-coated glass slide (the diameter of glass slide is 12 mm).³⁶ Then, the glass slides attaching cells were placed in a 24-well plate. The cells fixed with 4% paraformaldehyde for 20 min at room temperature after rinsing twice with PBS. To block nonspecific binding, PBS with 10% newborn bovine serum (NBS; Invitrogen) was applied to the cultures for 30 min at 37 °C. Then, the cells were incubated at 4 °C overnight with primary antibodies diluted with PBS (containing 0.2% Triton X-100 and 10% NBS). The primary antibodies used were as follows: monoclonal mouse anti-Epcam (1:50; Boster, Wuhan, China) and polyclonal rabbit anti-CD45 (1:50; Boster). After rinsing thrice with PBS, the cultures were incubated in PBS containing 5% NBS and either goat anti-mouse IgG-RBITC (1:20; Boster; and fluorescence was detected at 540/625 nm) or goat anti-rabbit IgG-FITC (1:20; Boster; and fluorescence was detected at 490/525 nm) secondary antibody at 37 °C for 2 h. Subsequently, the cultures were rinsed thrice with PBS and incubated for 10 min in PBS containing Hoechst dye (H33258 fluorochrome, 0.5 µg/mL; Sigma; fluorescence was detected at 365/460 nm). Before imaging, the cells were rinsed twice with PBS again.

Microscopy and image analysis

An inverted microscope (Olympus, CKX41) with a charge coupled device camera (Olympus, DP72) and a mercury lamp (Olympus, URFLT50) was used to obtain phase contrast and fluorescence images. Time-lapse images of the samples were obtained every 1 s. A total of 100 to 200 images were overlaid to create each averaged composite image. Image and data analyses were performed using Image-Pro[®] Plus 6.0 (Media Cybernetics, Silver Spring, MD) and SPSS 12.0 (SPSS Inc.) software, respectively. The results and error bars in the graphs are expressed as the mean ± SD.

Results and discussion

Distribution of different types of cells in the filter matrices

To preliminarily evaluate the capability of the device to separate cells with different deformability, the distribution of the three types of cells (MCF-7, MDA-MB-231 and MDA231-LM2) in the filter matrices was first observed, respectively. The three types of cells have no significant difference in the diameter (MCF-7 cells were 18.5±2.3 µm, MDA-MB-231 cells were 17.9±2.5 µm, and MDA231-LM2 cells were 17.5±1.9 µm). However, the mesenchymal-like cancer cell lines MDA-MB-231 and MDA231-LM2 showed greater deformability than the epithelium-like cancer cell line MCF-7.³⁷⁻³⁹ Therefore, in this study, MDA-MB-231 and MDA231-LM2 cells were used as the flexible cell model and MCF-7 cells were used as the less flexible cell model. Meanwhile, the 10-µm diameter green fluorescence microspheres were used as a rigid control. For easy visualization, MDA-MB-231 and MDA231-LM2 cells were stained red with Cell Tracker Orange CMRA and MCF-7 cells were stained green with Cell Tracker Green CMFDA.^{32,38}

Initially, the cell/microsphere sample (the cell density is 1×10⁶ cells/mL) was infused into the device from the cell inlet at a flow rate of 60 µL/min in 1-2 s to load 1 000 to 2 000 cells/microspheres. After that, the inlet channel was closed. Then, the sample was pushed by the driving buffer from L1 channel at a flow rate of 203 µL/min for 5 s; according to Eq. 1, the flow rate corresponded to the pressure drop of 6 kPa. The selection of the flow rate and the infusion time was according to the related studies reported previously.^{5,31} The forward biased flow enables the cells/microspheres to travel through the separation area of the device and were captured in the appropriate position of the filter matrices. Considering the number of the filter units in the filter matrices, 1×10³-2×10³ cells were sorted for each process. The cell number distributed in each filter matrix was counted manually under an optical microscope. For clarity and to compare with the rigid microspheres, the movements of the cells and the microspheres at the 10-µm filter matrix were recorded during the infusion, sorting and release processes (Fig. 2A, and Movie S3 and S4, ESI[†]). A direct observation of the images and the Movies showed that the rigid microspheres were well trapped at the entrance of the 10-µm filter matrix. The majority of MDA-MB-231 and MDA231-LM2 cells entered the 10-µm filter matrix. However, only a few MCF-7 cells were observed at this matrix. Statistical analysis (Fig. 2B) showed that the three types of cells were all obtained a narrow distribution in the filter matrices. MCF-7 cells were mainly distributed in the wide filter matrices (the pore size was 20-12 µm) with the percentage of 86.45%. MDA-MB-231 and MDA231-LM2 cells were mainly distributed in the narrow filter matrices (the pore size was 10-6 µm) with the percentage of 75.84% and 83.62%, respectively. However, 81.76% microspheres were only trapped at the first column of the 10-µm filter matrix. The distribution of cancer cells and microspheres are all correlated to the filter size. However, the correlation between the filter size and microsphere is more than the correlation between filter size and cancer cell. Because most of the cell filter size is smaller than the cell size, the cells were compressed more than the rigid microspheres under this sorting condition. Additionally, comparing the pore size of the filter matrices with the cell size,

MDA-MB-231 and MDA231-LM2 cells were compressed more than MCF-7 cells at the same flow rate during the sorting process. Due to the diameters of the three types of cells have no significant difference, the deformability of the cells likely made greater contribution to the cell distribution than the cell size.^{4,5} All the results demonstrated the potential of the device to sort cells and microspheres based on their size and deformability, expanding the current repertoire of the cell separation methods.

Optimization of the operating parameters

A characteristic, significant difference and stable cell distribution after sorting is very important for microstructure-constricted cell separation device, which will affect the cell separation rate.^{5,28,30,31} In this study, the cell distribution in the filter matrices after sorting was primarily governed by the two operating parameters: the flow rate and the duration time. To study the effect of the flow rate on the cell distribution, MCF-7, MDA-MB-231 and MDA231-LM2 cells were respectively sorted at different driving flow rates (203, 406, 609, 812, and 1015 $\mu\text{L}/\text{min}$) for 5 s in the filter matrices after they were introduced into the device. According to Eq.1, these flow rates respectively corresponded to the pressure drop 6, 12, 18, 24, and 32 kPa. Expectedly, the cells tended to distribute in the narrow filter matrices as the driving flow rate increasing, and high driving flow rate led to a wide cell distribution (Fig. S6A, ESI[†]). The results also indicated that the less flexible MCF-7 cell distribution tended to the narrow filter matrices as the flow rate increasing, resulting in the distributions of MCF-7 and the other two cells no significant difference. A comprehensive analysis showed that the MCF-7 cell distribution was great different with the MDA-MB-231 and MDA231-LM2 cells at the driving flow rate of 203 $\mu\text{L}/\text{min}$.

Using the same method, the effect of the duration time on the cell distribution was also investigated under different infusion times (2, 3, 4, 8 and 10 s) at the optimized driving flow rate of 203 $\mu\text{L}/\text{min}$. The results were shown in Fig. S6B (ESI[†]). The 2s duration time is too short to drive enough cells into the filter matrices. When the infusion time is 3-10 s, the three types of cells were well distribute in the different areas of the filter matrices: MCF-7 cells were mainly distributed in the wide filter matrices (the pore size was 20-12 μm) and MDA-MB-231 and MDA231-LM2 cells were mainly distributed in the narrow filter matrices (the pore size was 10-6 μm). Therefore, 3 s was chosen as the optimized duration time for cell infusion during the sort process.

Considering the stability and repeatability of the device under the optimized conditions, 5 round trials were conducted on different days using different devices. As shown in Fig. S7 (ESI[†]), the resulting distributions were consistent and repeatable. Moreover, cell viability analysis (Fig. S8, ESI[†]) showed that the separation process does not compromise cell viability (>93%) and the morphology and proliferation rate of the sorted cells were analogous to the control cells (Fig. S9, ESI[†]), no noticeable changes were observed. The recovery efficiency of the sorted cells was more than 95% (Fig. S10, ESI[†]). Therefore, the driving flow rate of 203 $\mu\text{L}/\text{min}$ and the duration time of 3 s were used in the subsequent studies.

Separation of cell mixtures with different deformability

To evaluate the ability of the device to separate cells with different deformability from a cell mixture, two kinds of cell mixtures (MCF-7 and MDA-MB-231 cells, and MCF-7 and MDA231-LM2 cells) were separated under the optimized condition. The less flexible cells (MCF-7, stained with green fluorescence) and the flexible cells (MDA-MB-231/MDA231-LM2, stained with red fluorescence) were cultured separately. Then, MCF-7 and MDA-MB-231 (or MDA231-LM2) cells were mixed in equal amounts with a final density of 1×10^6 cells/mL. Afterward, the cell mixtures were separated using the methods described above. The cell distribution after sorted in the filter matrices was shown in Fig. S11 and Fig. S12 (ESI[†]). Considering the different cell distributions of the less flexible cells and the flexible cells in the filter matrices, the filter matrices were divided into two parts: the wide filter matrices (the pore size was 20-12 μm) and the narrow filter matrices (the pore size was 10-6 μm). Generally, the less flexible cells MCF-7 were mainly distributed in the wide filter matrices, while the flexible cells MDA-MB-231/MDA231-LM2 were mainly distributed in the narrow filter matrices. This result was consistent with the sort of the single type of cells (Fig. S7, ESI[†]). It should be noted that cellular heterogeneity does exist within the cell types and affects the quality of the separation.^{5,27,34} Specifically, a proportion of less flexible cells passed through the wide filter matrices and were trapped in the narrow filter matrices, and some flexible cells retained in the wide filter matrices. This phenomenon can be also observed from the cell images before and after separation (Fig. 3A and B).

Further analysis of each cell fraction in the collected cells (Fig. 3C and D) showed that in the separation of MCF-7 and MDA231-LM2 cell mixture, the fraction of MCF-7 cells increased from the original 50% to 81.3% at the wide filter matrices, and MDA231-LM2 increased from 50% to 84.7% at the narrow filter matrices. In the separation of the MCF-7 and MDA-MB-231 cell mixture, the fraction of MCF-7 cells increased from 50% to 75.1% at the wide filter matrices, and MDA231-LM2 increased from 50% to 78.6% at the narrow filter matrices. Compared with the previous separation of cancer cell,⁵ this device showed high purity for these different cancer cells, indicating that the device could be used to separate less flexible cells and flexible cells for the study on the cancer metastatic and cancer-initiating. Additionally, the result showed that the separation efficiency of the MCF-7 and MDA231-LM2 mixture is better than the MCF-7 and MDA-MB-231 mixture. The reason may be that MDA231-LM2 cells are likely to have more deformability than MDA-MB-231 cells, since the potential metastasis of MDA231-LM2 cells was greater than MDA-MB-231 cells.³⁷⁻³⁹

Separation of cancer cells from blood samples

The separation of rare cells (e.g., circulating tumor cells, CTCs) from the peripheral blood is an interesting topic for the study of tumor diagnosis and therapy.²⁷ In this study, the separation of cancer cells from blood samples was also investigated by

spiking cancer cells into the whole blood. Generally, human blood is composed of the following three main types of cells: erythrocytes, leukocytes and platelets. Erythrocytes or RBCs are discoid biconcave shaped cells with diameters ranging from 6 μm to 8.5 μm and thicknesses ranging from 1.8 μm to 2.8 μm . Leukocytes or WBCs are nearly spherical cells with diameters larger than 6 μm to 10 μm . Platelets have diameters ranging from 1 μm to 3 μm .³² Additionally, erythrocytes and leukocytes are highly deformable. Therefore, the microfluidic system could offer a potential application for rare cell separation according to previous studies.^{28,30} In this experiment, human whole blood drawn from healthy volunteers was collected in ethylene-diaminetetra acetic acid vacuum tubes and diluted by the buffer (PBS, 0.01 mol/L, PH 7.4; citric acid, 4.8 g/L; trisodium citrate, 13.2 g/L; and dextrose, 14.7 g/L) with a volume ratio of 1:4, corresponding to the hematocrit value of 8% and erythrocyte density of 1×10^9 cells/mL. After that, cancer cells (i.e., MCF-7, MDA-MB-231 or MDA231-LM2) were spiked into the diluted blood samples with a cancer cell-to-blood cell ratio of $1/10^6$. The blood samples containing different cancer cells were then isolated in the device.

To obtain high separation purity of the cancer cells, blood cells should be excluded through the waste outlet as much as possible, and the mixed cancer cells should be recovered through the cell outlet as much as possible. Thus, the collection efficiency of blood cells and cancer cells were first evaluated. Considering the continuous opening of the cell inlet during the cancer cell separation from blood samples, the cancer cell suspension (1×10^3 cells/mL) or diluted blood (1×10^9 erythrocyte/mL) was separately infused into the device from the cell inlet at different flow rates (10, 20, 40, 60, 80 and 100 $\mu\text{L}/\text{min}$). Simultaneously, the L1 channel was opened to allow the buffer (203 $\mu\text{L}/\text{min}$) to drive the cancer cells/blood through the filter matrices. The results (Fig.S13, ESI†) showed that the collection efficiency of the trapped cancer cells in the filter matrices had an inverse relationship with the input flow rate of the cell suspension, and the number of the trapped blood cells had a proportional relationship with the input flow rate of the blood sample. The reason is that the blood cell number entered the device increasing with the high flow rate. In addition, more blood cells attempted to occupy the same pore positions spontaneously, resulting in enhanced cell–cell interaction and the consequent blood cell aggregates, which made the number of trapped blood cells increase.²⁸ However, the cell–cell interaction and the consequent cell aggregates caused the cancer cell collection efficiency decrease due to their large diameter size as well as the relative strong cell–cell interactions.^{5,31–32} At the flow rates of 10 and 20 $\mu\text{L}/\text{min}$, the collection efficiency of cancer cells was more than 95%, and the number of blood cells trapped in the filter matrices was less than 100 cells/mL. When the flow rate was more than 40 $\mu\text{L}/\text{min}$, the collection efficiency of cancer cells was less than 90%, and the number of blood cells trapped in the filter matrices was more than 500 cells/mL. Considering both the throughput and the recovery performance, the flow rate of 40 $\mu\text{L}/\text{min}$ was employed to introduce cell/blood samples into the device in the separation of cancer cells from the spiked blood

samples. At this flow rate, the collection efficiency of the three types of cancer cells was in the range of 90% to 95%, and the number of trapped blood cells was less than 250 cells/mL.

To carry out the separation of cancer cells from the whole blood, mimicking the isolation of rare cells from human peripheral blood, the fluorescence labeled cancer cells MCF-7, MDA-MB-231 or MDA231-LM2 ($\sim 1 \times 10^4$ cells) were mixed with diluted whole blood (~ 10 mL) at a final cancer cell-to-blood cell ratio of $1/10^6$. Then, the cancer cell-contained blood was infused into the device through the cell inlet (40 $\mu\text{L}/\text{min}$) along with the driving buffer from L1 channel (203 $\mu\text{L}/\text{min}$). In this study, to facilitate data analysis, the filter matrices were also divided into the wide filter matrices (the pore size was 20–12 μm) and the narrow filter matrices (the pore size was 10–6 μm). Collection of the trapped cells was performed at the outlets every half hour to avoid cell aggregates in the filter matrices. Figs. 4A, S14 and S15 (ESI†) typically showed the cell movements during the infusion, sorting and exclusion processes at the 10- μm (narrow) and 14- μm (wide) filter matrices. A direct comparison of these images (especially the fluorescence images) showed that cancer cells could be trapped in the filter matrices. The less flexible MCF-7 cells were mainly in the 14- μm (wide) filter matrix, and the flexible cancer MDA-MB-231 and MDA231-LM2 cells were in the 10- μm (narrow) filter matrix. However, the blood cells with small size could not be captured in the two filter matrices. MDA231-LM2 cell separation at 10- μm filter matrix was shown in Movie S5 (ESI†), which clearly presented the whole processes, including the cell infusion, sorting and exclusion.

In this experiment, three parameters were selected to assess the separation efficiency of the microdevice, including cell recovery efficiency, purity and viability. As shown in Fig. 4B, the recovery efficiency of MCF-7, MDA-MB-231 and MDA231-LM2 cells was $94.2 \pm 3.3\%$, $91.1 \pm 4.0\%$ and $90.0 \pm 4.9\%$, respectively. Among them, the collection efficiency of the less flexible cancer MCF-7 cells was greater than the flexible cancer cells (MDA-MB-231 and MDA231-LM2), which was consistent with the independent isolation experiment above. The results indicated that the vast majority of the cancer cells spiked in the whole blood were isolated through the device. To evaluate the cell purity, the collected cancer cells were divided into two parts according to the pore sizes (the wide filter matrices, 20–12 μm ; and the narrow filter matrices, 10–6 μm), because of the different deformability between the less flexible cancer cells (MCF-7) and the flexible cancer cells (MDA-MB-231 and MDA231-LM2). Fig. S16 (ESI†) is the representative images of the cancer cells collected from the wide (20–12 μm) and narrow (10–6 μm) filter matrices, which clearly showed the separation efficiency of the microdevice by comparison with the initial cell sample and the cells collected from the waste outlet. Quantitative analysis (Fig. S17, ESI†) showed that the purity of the cancer cells collected from wide (20–12 μm) filter matrices was $96.1 \pm 4.1\%$ (MCF-7), $93.7 \pm 5.9\%$ (MDA-MB-231) and $92.9 \pm 6.2\%$ (MDA231-LM2). For the cells collected from the narrow (10–6 μm) filter matrices, the purity was $77.7 \pm 5.5\%$ (MCF-7), $75.8 \pm 8.6\%$ (MDA-MB-231) and $73.8 \pm 8.0\%$ (MDA231-LM2). The purity of the cells

collected from the narrow (10-6 μm) filter matrices is less than those from the wide (20-12 μm) filter matrices. The reason is that the blood cells were able to pass through the 20-12 μm filter matrices due to their small size, while some leukocytes could be trapped in the 10-6 μm filter matrices because the pore size was similar with the big leukocytes.³¹ A comprehensive analysis (Fig. 4C) by combining all the cells collected from the narrow and wide filter matrices showed that the cell purity was 87.6 \pm 5.4% (MCF-7), 82.6 \pm 5.9% (MDA-MB-231) and 80.9 \pm 6.1% (MDA231-LM2). Considering the recovered cells may contain some blood cells, the amount of cancer cells in all the collected cells were also analyzed in the current study by using immunofluorescence assay.⁴⁰ The cancer cells were defined as EpCAM+/CD45- with red fluorescence and leukocytes were identified as EpCAM-/CD45+ with green fluorescence.²² Fig. 5A showed the typical bright field and fluorescence images of the cancer cells and leukocytes in the collected cells. Quantitative analysis (Fig. 5B) showed that the cancer cells accounted for 85.8 \pm 4.43% (MCF-7), 80.34 \pm 3.6% (MDA-MB-231) and 79.2 \pm 4.7% (MDA231-LM2). The results were consistent with the CellTracker-labeled experiments, further verifying the recovered cancer cells have high purity.

Cell viability and integrity assays by using the AO/PI double-staining protocol and re-culture showed that the viabilities of the collected cancer cells were all more than 92% (Fig. S18, ESI[†]) with good morphology and proliferation ability, and no noticeable changes were observed by comparison with the common bench top control cells (Figs. 6 and S19, ESI[†]), indicating that the separation process does not compromise cell viability and integrity. Compared these results with the current filtration methods (Table S1, ESI[†]), the device possess the potential to separate rare cells with high collection recovery and purity.

Conclusions

In this work, we presented an integrated microfluidic device for continuous sort and separation of cancer cells by combining funnel-like filter matrices and the microvalve system. The flow dynamics around the filter was carefully analyzed by numerical simulation and the operating parameters were optimized. Separation of cancer cells (MCF-7, MDA-MB-231 and MDA231-LM2) with different deformability showed that the mixture of the less flexible cells (MCF-7) and the flexible cells (MDA-MB-231 and MDA231-LM2) can be well separated with more than 75% purity. Moreover, the device can be employed to separate cancer cells from the blood samples with more than 90% cell recovery and more than 80% purity. Compared with the current filtration methods, the device provide a new approach for cancer cell separation with high collection recovery and purity, also, it possess practical potential to be applied as a sample preparation platform for fundamental studies and clinical applications. However, the throughput of this device is limited by the small separation area, which may be improved by enlarging the separation area and parallelizing the filter matrices. The further improvement of the current device and its application to separate actual

clinical samples were under way in our laboratory by cooperation with tumor research institutes.

Acknowledgements

This study was supported by the National Natural Science Foundation of China (21375106 and 21175107), the Ministry of Education of the People's Republic of China (NCET-08-602 0464), the Fundamental Research Funds for the Central Universities (Z109021303), the Scientific Research Foundation for the Returned Overseas Chinese Scholars, the State Education Ministry, and Northwest A&F University.

Notes and references

- C. M. E. Myrand-Lapierre, X. Deng, R. R. Ang, K. Matthews, A. T. Santoso and H. Ma, *Lab on a Chip*, 2015, **15**, 159-167.
- P. S. Knoepfler, *Stem Cells*, 2009, **27**, 1050-1056.
- J. A. Thomson, J. Itskovitz-Eldor, S. S. Shapiro, M. A. Waknitz, J. J. Swiergiel, V. S. Marshall and J. M. Jones, *Science*, 1998, **282**, 1145-1147.
- W. C. Lee, H. Shi, Z. Y. Poon, L. M. Nyan, T. Kaushik, G. V. Shivashankar, J. K. Y. Chan, C. T. Lim, J. Han and K. J. Van Vliet, *Proceedings of the National Academy of Sciences of the United States of America*, 2014, **111**, E4409-E4418.
- W. J. Zhang, K. Kai, D. S. Choi, T. Iwamoto, Y. H. Nguyen, H. L. Wong, M. D. Landis, N. T. Ueno, J. Chang and L. D. Qin, *Proceedings of the National Academy of Sciences of the United States of America*, 2012, **109**, 18707-18712.
- M. Yu, A. Bardia, N. Aceto, F. Bersani, M. W. Madden, M. C. Donaldson, R. Desai, H. L. Zhu, V. Comaill, Z. L. Zheng, B. S. Wittner, P. Stojanov, E. Brachtel, D. Sgroi, R. Kapur, T. Shioda, D. T. Ting, S. Ramaswamy, G. Getz, A. J. Iafrate, C. Benes, M. Toner, S. Maheswaran and D. A. Haber, *Science*, 2014, **345**, 216-220.
- X. Tang, T. B. Kuhlenschmidt, Q. Li, S. Ali, S. Lezmi, H. Chen, M. Pires-Alves, W. W. Laegreid, T. A. Saif and M. S. Kuhlenschmidt, *Molecular Cancer*, 2014, **13**.
- D. Wirtz, K. Konstantopoulos and P. C. Searson, *Nature Reviews Cancer*, 2011, **11**, 512-522.
- V. Swaminathan, K. Mythreye, E. T. O'Brien, A. Berchuck, G. C. Blobe and R. Superfine, *Cancer Research*, 2011, **71**, 5075-5080.
- C. W. Shields Iv, C. D. Reyes and G. Lopez, *Lab on a Chip*, 2015.
- J. Pruszk, K. C. Sonntag, M. H. Aung, R. Sanchez-Pernaute and O. Isacson, *Stem Cells*, 2007, **25**, 2257-2268.
- W. R. Jones, H. P. Ting-Beall, G. M. Lee, S. S. Kelley, R. M. Hochmuth and F. Guilak, *Journal of Biomechanics*, 1999, **32**, 119-127.
- S. Riethdorf, H. Fritsche, V. Muller, T. Rau, C. Schindibeck, B. Rack, W. Janni, C. Coith, K. Beck, F. Janicke, S. Jackson, T. Gornet, M. Cristofanilli and K. Pantel, *Clinical Cancer Research*, 2007, **13**, 920-928.
- M. Mego, S. A. Mani, C. Li, E. Andreoupolou, S. Tin, S. Jackson, E. N. Cohen, H. Gao, M. Cristofanilli and J. M. Reuben, *Cancer Research*, 2009, **69**, 649S-650S.
- K. D. Costa, *Disease Markers*, 2003, **19**, 139-154.
- M. Lekka and P. Laidler, *Nature Nanotechnology*, 2009, **4**, 72-72.
- J. Y. Wang, Z. F. Wan, W. M. Liu, L. Li, L. Ren, X. Q. Wang, P. Sun, L. L. Ren, H. Y. Zhao, Q. Tu, Z. Y. Zhang, N. Song and L. Zhang, *Biosensors & Bioelectronics*, 2009, **25**, 721-727.
- B. Eckes, D. Dogic, E. Colucci-Guyon, N. Wang, A. Maniotis, D. Ingber, A. Merckling, F. Langa, M. Aumailley, A. Delouvee, V. Kotliansky, C. Babinet and T. Krieg, *Journal of Cell Science*, 1998, **111**, 1897-1907.
- R. A. Harouaka, M. Nisic and S. Y. Zheng, *Jala*, 2013, **18**, 455-468.
- A. Alazzam, I. Stiharu, R. Bhat and A. N. Meguerditchian, *Electrophoresis*, 2011, **32**, 1327-1336.

Paper

Analyst

- 1
2
3
4
5
6
7
8
9
10
11
12
13
14
15
16
17
18
19
20
21
22
23
24
25
26
27
28
29
30
31
32
33
34
35
36
37
38
39
40
41
42
43
44
45
46
47
48
49
50
51
52
53
54
55
56
57
58
59
60
- 21 H. Song, J. Rosano, Y. Wang, C. Garson, B. Prabhakarpanid, K. Pant, G. Klarmann, A. Perantoni, L. Alvarez and E. Lai, *Lab on a Chip*, 2015, DOI: 10.1039/C4LC01253D.
- 22 H. W. Hou, M. E. Warkiani, B. L. Khoo, Z. R. Li, R. A. Soo, D. S. W. Tan, W. T. Lim, J. Han, A. A. S. Bhagat and C. T. Lim, *Scientific Reports*, 2013, DOI: 10.1038/srep01259.
- 23 E. Sollier, D. E. Go, J. Che, D. R. Gossett, S. O'Byrne, W. M. Weaver, N. Kummer, M. Rettig, J. Goldman, N. Nickols, S. McCloskey, R. P. Kulkarni and D. Di Carlo, *Lab on a Chip*, 2014, **14**, 63-77.
- 24 J. S. Sun, M. M. Li, C. Liu, Y. Zhang, D. B. Liu, W. W. Liu, G. Q. Hu and X. Y. Jiang, *Lab on a Chip*, 2012, **12**, 3952-3960.
- 25 T. Huang, C. P. Jia, Y. Jun, W. J. Sun, W. T. Wang, H. L. Zhang, H. Cong, F. X. Jing, H. J. Mao, Q. H. Jin, Z. Zhang, Y. J. Chen, G. Li, G. X. Mao and J. L. Zhao, *Biosensors & Bioelectronics*, 2014, **51**, 213-218.
- 26 J. S. Kuo, Y. X. Zhao, P. G. Schiro, L. Y. Ng, D. S. W. Lim, J. P. Shelby and D. T. Chiu, *Lab on a Chip*, 2010, **10**, 837-842.
- 27 W. Beattie, X. Qin, L. Wang and H. S. Ma, *Lab on a Chip*, 2014, **14**, 2657-2665.
- 28 B. K. Lin, S. M. McFaul, C. Jin, P. C. Black and H. S. Ma, *Biomicrofluidics*, 2013, DOI: 10.1063/1.4812688.
- 29 S. Y. Zheng, H. K. Lin, B. Lu, A. Williams, R. Datar, R. J. Cote and Y. C. Tai, *Biomedical Microdevices*, 2011, **13**, 203-213.
- 30 P. Pereira, V. Grandne, J. M. Forel, S. Gabriele, M. Camara and O. Theodoly, *Lab on a Chip*, 2013, **13**, 161-170.
- 31 S. M. McFaul, B. K. Lin and H. S. Ma, *Lab on a Chip*, 2012, **12**, 2369-2376.
- 32 S. F. Shen, C. Ma, L. Zhao, Y. L. Wang, J. C. Wang, J. Xu, T. B. Li, L. Pang and J. Y. Wang, *Lab on a Chip*, 2014, **14**, 2525-2538.
- 33 J. Y. Wang, G. D. Sui, V. P. Mocharla, R. J. Lin, M. E. Phelps, H. C. Kolb and H. R. Tseng, *Angewandte Chemie-International Edition*, 2006, **45**, 5276-5281.
- 34 Y. D. Tang, J. Shi, S. S. Li, L. Wang, Y. E. Cayre and Y. Chen, *Scientific Reports*, 2014, DOI: 10.1038/srep06052
- 35 W. C. Lee, A. A. S. Bhagat, S. Huang, K. J. Van Vliet, J. Han and C. T. Lim, *Lab on a Chip*, 2011, **11**, 1359-1367.
- 36 N. M. Karabacak, P. S. Spuhler, F. Fachin, E. J. Lim, V. Pai, E. Ozkumur, J. M. Martel, N. Kojic, K. Smith, P. I. Chen, J. Yang, H. Hwang, B. Morgan, J. Trautwein, T. A. Barber, S. L. Stott, S. Maheswaran, R. Kapur, D. A. Haber and M. Toner, *Nature Protocols*, 2014, **9**, 694-710.
- 37 I. Y. Wong, S. Javaid, E. A. Wong, S. Perk, D. A. Haber, M. Toner and D. Irimia, *Nature Materials*, 2014, **13**, 1063-1071.
- 38 A. J. Liu, W. M. Liu, Y. L. Wang, J. C. Wang, Q. Tu, R. Liu, J. Xu, S. F. Shen and J. Y. Wang, *Microfluidics and Nanofluidics*, 2013, **14**, 515-526.
- 39 M.-Y. Kim, T. Oskarsson, S. Acharyya, D. X. Nguyen, X. H.-F. Zhang, L. Norton and J. Massagué, *Cell*, 2009, **139**, 1315-1326.
- 40 C. Wyatt Shields Iv, C. D. Reyes and G. P. Lopez, *Lab on a Chip*, 2015, DOI: 10.1039/C4LC01246A.

Captions to Figures

Fig. 1 Integrated microfluidic system for cell separation based on different size and deformation. (A) Schematic diagram of the design of the microdevice. The various channels were showed with different colored to help visualize the different components of the microfluidic device. Green indicates the fluidic channels and red indicates the valves. The separation area (1500 μm wide, 25 μm high and 7000 μm long) contained 8-group funnel-like filter matrices for cell sorting. The distance between the two neighbouring filter units was decided by the pore size, which was constant in each matrix, but decreased in the subsequent matrices with a decrement of 2 μm from 20 to 6 μm . L1, L2, L3, L4 and L5 channels were used for the buffer infusion. (B) An actual image of the device with dimensions of 3.0 cm \times 3.0 cm. (C) Schematic diagram of the operational cycle of cell separation in the separation area. The cell separation device operates on a repeating three-step cycle of infusion, sorting and exclusion.

Fig. 2 (A) Fluorescence images of the microspheres and cancer cells in the 10- μm filter matrix during microsphere/cell infusion, sorting and exclusion processes. For easy visualization, MDA-MB-231 and MDA231-LM2 cells were stained red with Cell Tracker Orange CMRA and MCF-7 cells were stained green with Cell Tracker Green CMFDA before infusion. The white arrows showed the trajectories of microspheres and cells. The area between 10- μm filter matrix and the valve located between the 12- μm and 10- μm filter matrices was marked with two blue dotted lines. The separation process of the microspheres and MDA231-LM cells were shown in Movie S3 and S4 (ESI[†]). Scale bar, 100 μm . (B) The distribution of microsphere and cancer cell in the 8-group filter matrices after sorting process.

Fig. 3 (A) Representative cell images before and after the separation of MCF-7 and MDA231-LM2 cell mixture. Both bright-field and fluorescence images were presented. The image of initial cells showed approximately equal numbers of two types of cells (the first column). The image of the cancer cells (MCF-7 and MDA231-LM2) collected from the wide (20-12 μm) and narrow (10-6 μm) filter matrices showed a significantly enriched population of the two types of cells (the second and third columns). (B) Representative cell images before and after the separation of MCF-7 and MDA-MB-231 cell mixture. Both bright-field and fluorescence images were presented. The image of initial cells showed approximately equal numbers of two types of cells (the first column). The image of the cancer cells (MCF-7 and MDA231-LM2) collected from the wide (20-12 μm) and narrow (10-6 μm) filter matrices also showed a significantly enriched population of the two types of cells (the second and third columns). (C) The bar graph displayed the proportion of MCF-7 and MDA231-LM2 cells before and after the separation of MCF-7 and MDA231-LM2 cell mixture. (D) The bar graph showed the proportion of MCF-7 and MDA-MB-231 cells before and after the separation of MCF-7 and MDA-MB-231 cell mixture. Values represent mean \pm SD from ten independent experiments by analyzing 200–300 cells each.

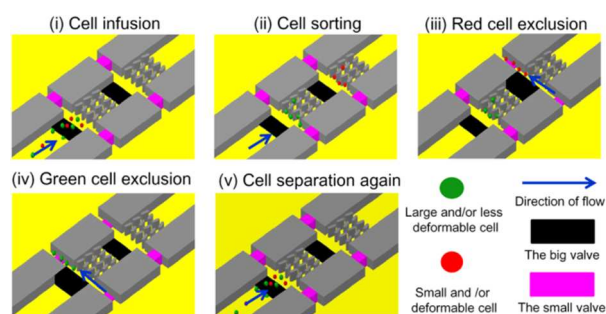
Fig. 4 Evaluation of the device to separate cells based on their different sizes and deformability by using cells MCF-7, MDA-MB-231 and MDA231-LM2. (A) The typical images of MDA231-LM2 cell-contained blood sample separation during the infusion, sorting and exclusion processes in the 10- μm filter matrix (the pore size is 10 μm). For easily distinguishing from blood cells, MDA231-LM2 cells were stained red with Cell Tracker Orange CMRA before the separation experiment. The cancer cells were mixed separately with blood samples at a final cancer cell-to-blood cell ratio of 1/10⁶. The big valve located between the 12- μm and 10- μm filter matrices were on the left (red or blue dotted line). The separation process of MDA231-LM2 cells in the 10- μm filter matrix was shown in Movie S5 (ESI[†]). (B) Collection efficiency of the three types of cancer cells (MCF-7, MDA-MB-231 and MDA231-LM2 cells) during the separation of cancer cell-contained blood samples. (C) Purity of the three types of cancer cells (MCF-7, MDA-MB-231 and MDA231-LM2 cells) separated from the blood samples. Standard deviations deduced from ten parallel experiments were shown as the error bars.

Fig. 5 Quantitative analysis of the purity of the recovered cancer cells (MCF-7, MDA-MB-231 and MDA231-LM2 cells) by using immunofluorescence assay. (A) The typical bright field and fluorescence images of the recovered cancer cells and leukocyte. EpCAM was stained with red fluorescence

(cancer cells), CD45 was stained with green fluorescence (Leukocytes) and Hoechst dye for nuclei identification. (B) Histogram plot of the purity of the recovered cancer cells (MCF-7, MDA-MB-231 and MDA231-LM2 cells) by using immunofluorescence assay. The results confirmed that the purity of the recovered cancer cells was basically consistent with the Cell Tracker-labelled experiments, further verifying that the recovered cancer cells possessed high purity. Standard deviations deduced from ten parallel experiments were shown as the error bars.

Fig. 6 Cellular viability assay of the three types of cancer cells (MCF-7, MDA-MB-231 and MDA231-LM2 cells) separated from blood samples by reseeded them back for 48 h culture. Before the experiment, MDA-MB-231 and MDA231-LM2 cells were stained red with Cell Tracker Orange CMRA and MCF-7 cells were stained green with Cell Tracker Green CMFDA. The images of cultures of control (unseparated) cells were also given and shown in Fig. S19 (ESI[†]).

Graphic abstract



We present an integrated microfluidic device for cell separation based on cell size and deformability by combining the microstructure-constricted filtration and pneumatic microvalves.

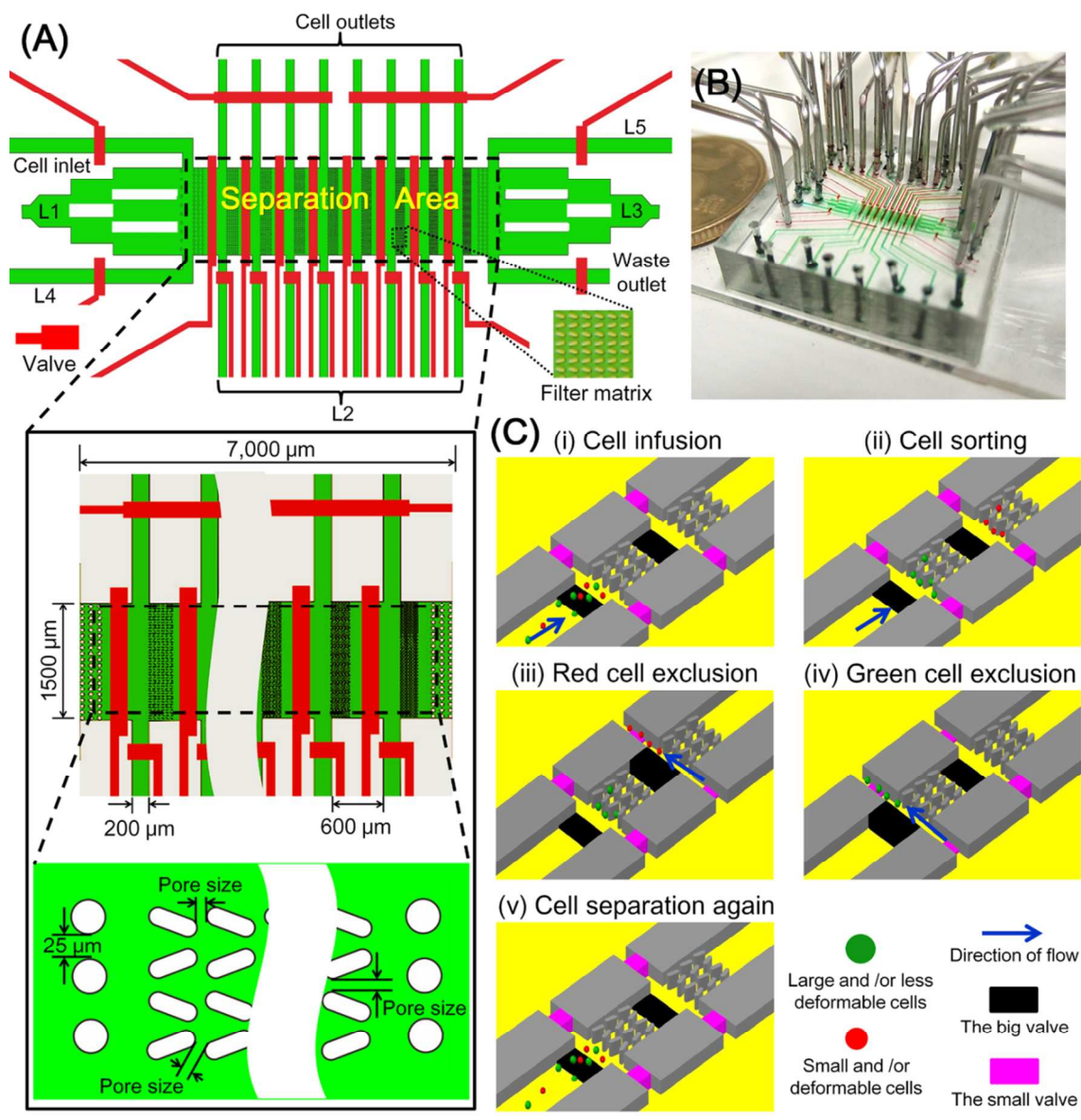


Figure 1

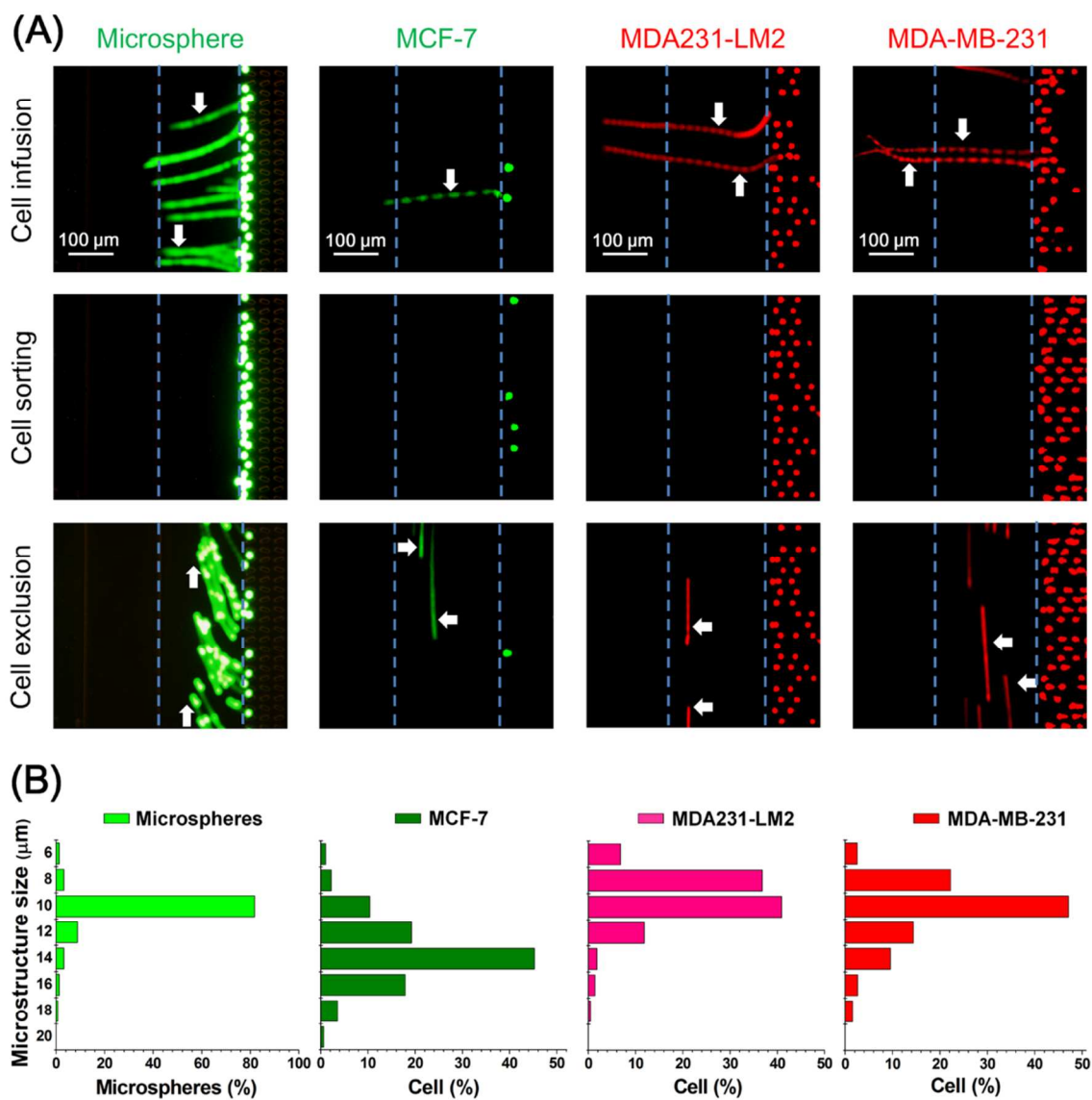


Figure 2

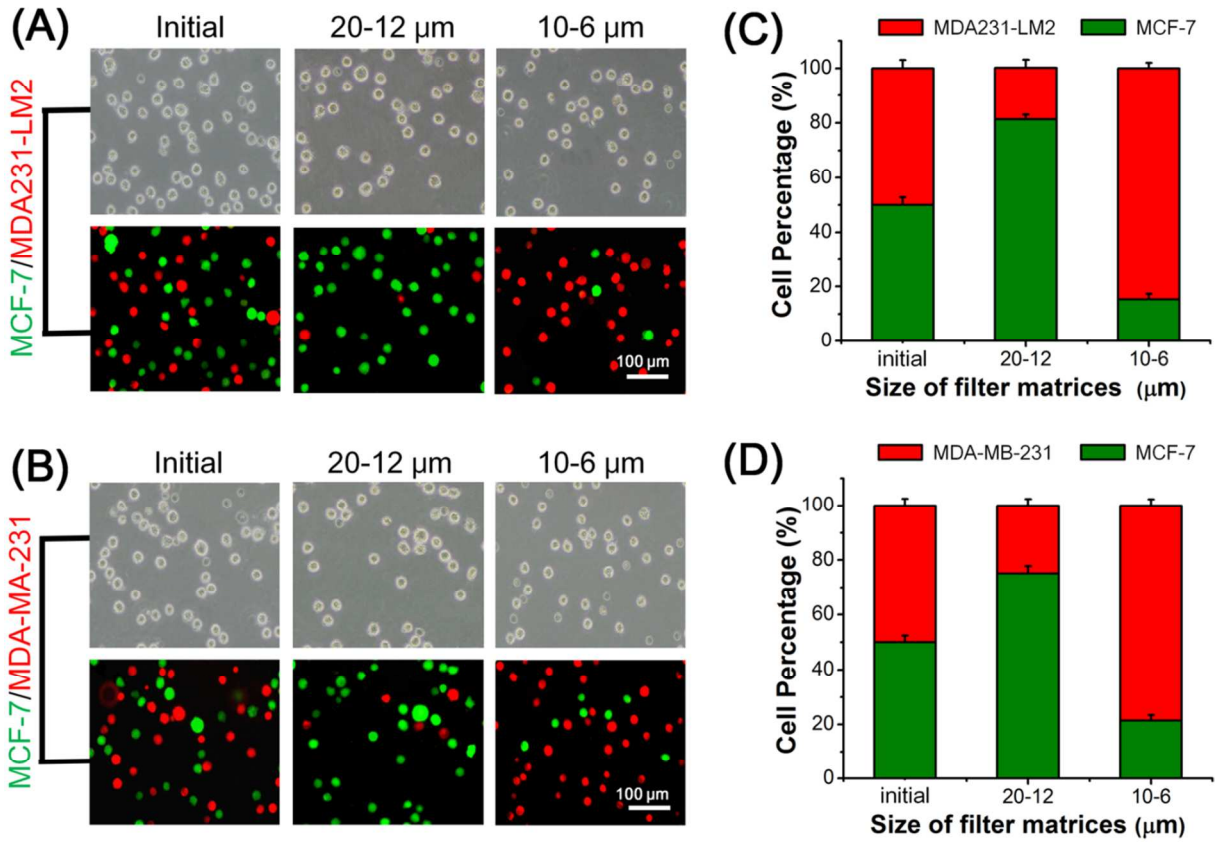


Figure 3

1
2
3
4
5
6
7
8
9
10
11
12
13
14
15
16
17
18
19
20
21
22
23
24
25
26
27
28
29
30
31
32
33
34
35
36
37
38
39
40
41
42
43
44
45
46
47
48
49
50
51
52
53
54
55
56
57
58
59
60

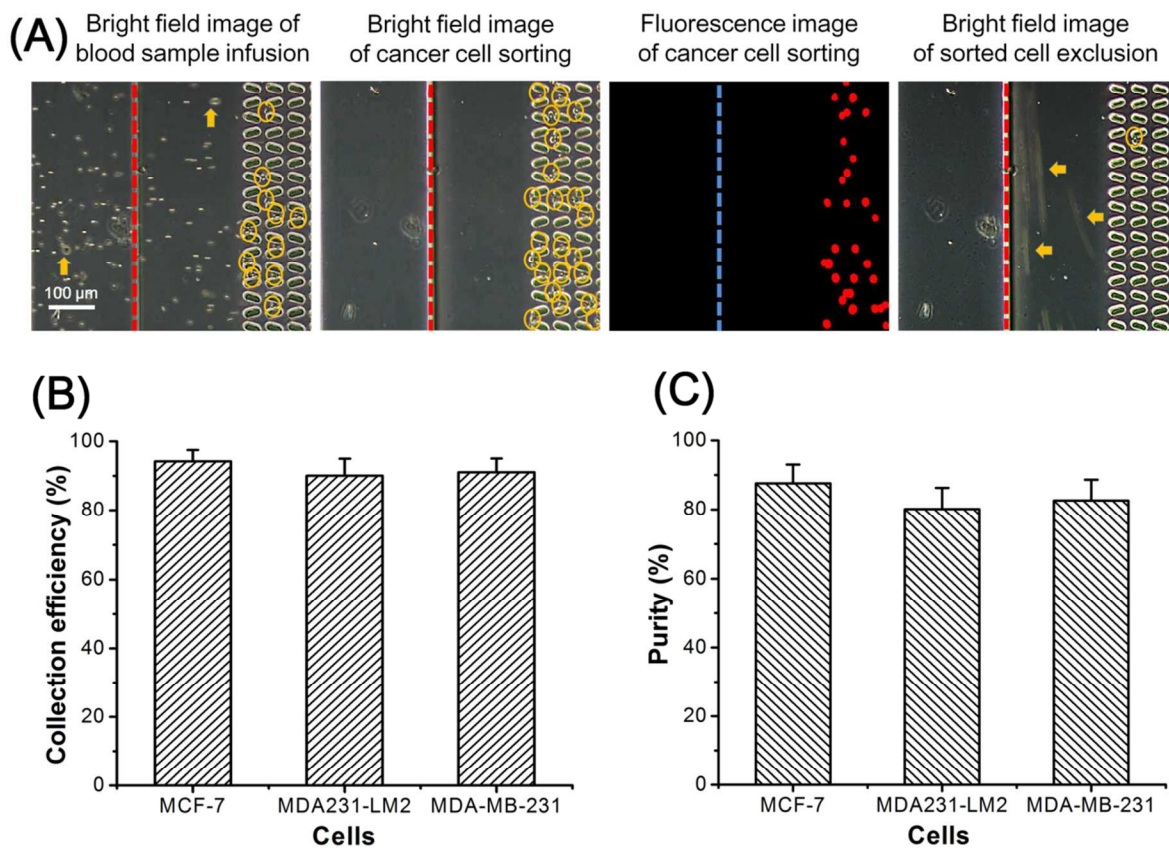


Figure 4

1
2
3
4
5
6
7
8
9
10
11
12
13
14
15
16
17
18
19
20
21
22
23
24
25
26
27
28
29
30
31
32
33
34
35
36
37
38
39
40
41
42
43
44
45
46
47
48
49
50
51
52
53
54
55
56
57
58
59
60

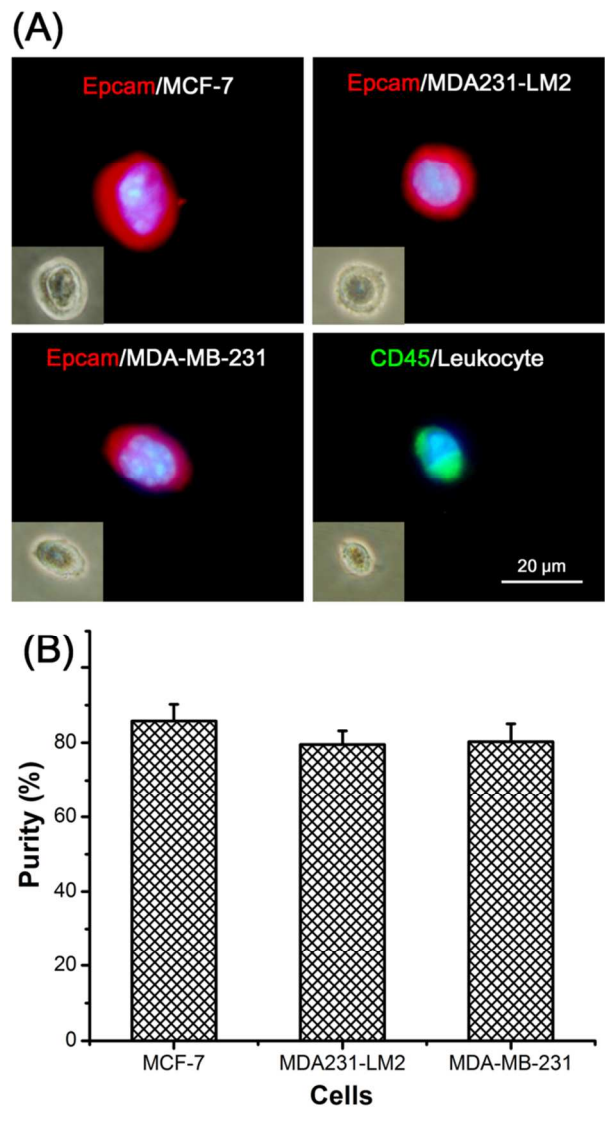


Figure 5

Analyst Accepted Manuscript

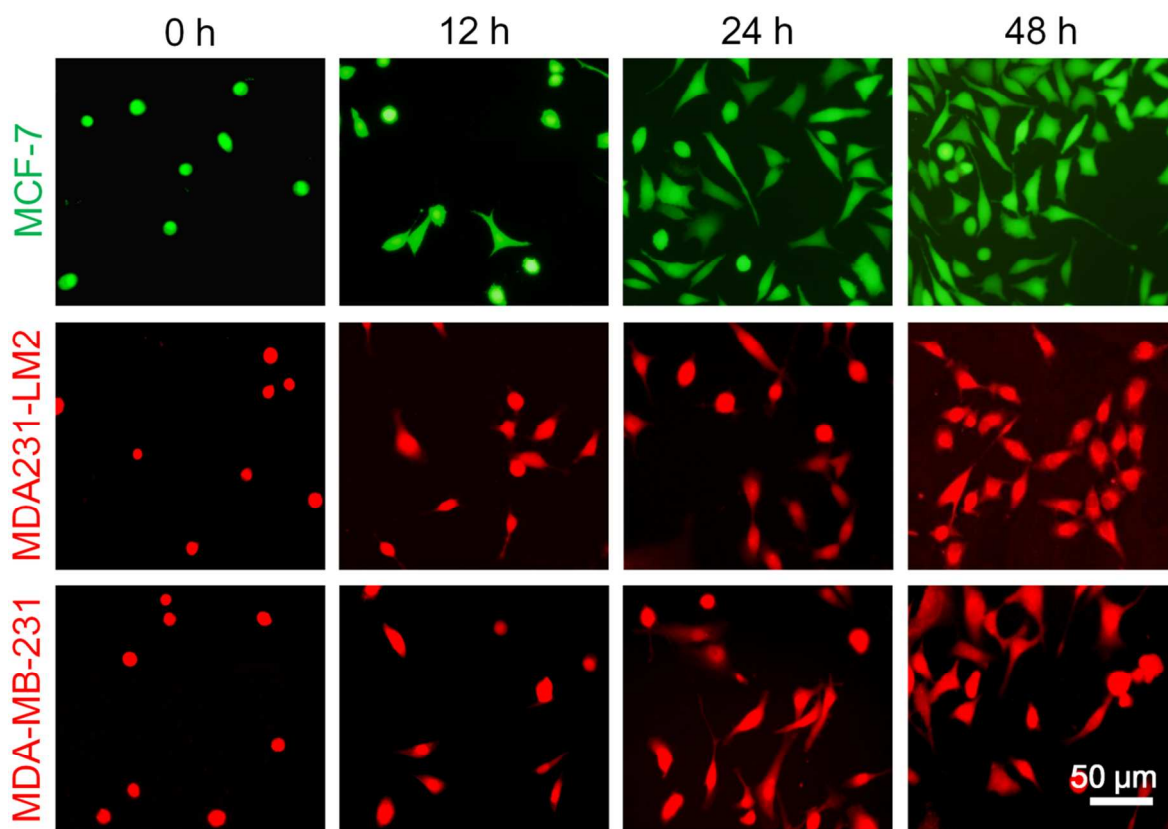


Figure 6